A SURVEY OF CLASSICAL AND NEW FINITE ELEMENT METHODS FOR THE COMPUTATION OF CRYSTALLINE MICROSTRUCTURE

MATTHIAS K. GOBBERT[1] AND ANDREAS PROHL[2]

Abstract. Recently, a geometrically nonlinear continuum theory has been developed for the equilibria of martensitic crystals based on elastic energy minimization. For these non-convex functionals, typically no classical solution exists, and minimizing sequences involving Young measures are studied. This paper presents an extensive computational survey of finite-element discretizations designed for this non-convex minimization problem supporting theoretical results previously obtained by the authors. Case studies for non-convex prototype problems are shown that compare the performance of three finite elements: conforming, classical non-conforming, and discontinuous finite elements. Both classical elements yield solutions that depend heavily on the underlying numerical mesh. The discontinuous finite element method overcomes this problem and shows optimal convergence behavior independent of the numerical mesh.

Key words. Ericksen-James energy density, finite element method, non-convex minimization, nonlinear conjugate gradients, multi-well problem, nonlinear elasticity, materials science.

AMS subject classifications. 49M07, 65K10, 65N30, 73C50, 73S10.

1 Introduction. Many new materials of interest in materials science and structural mechanics have been found to exhibit microstructure under certain ambient conditions. For example, certain alloys show laminate microstructure that can be observed in laboratory experiments [1, 2]. The understanding of these microscopic phenomena plays an important role to improve certain material properties like shape-memory, ferroelectricity, or magnetostriction, used for instance in micromachines.

A mathematical model for such "smart materials" was first given by Ball and James, [1, 2]. In there, minimizing solutions represent deformations that exhibit microstructures which are observed in experiments. A particular example is the phenomenon of twinning associated with austenite-martensite transformations [1, 2].

Because of the non-(quasi-)convex nature of the so-called Ericksen-James energy density, the related functional is not weakly lower semicontinuous and hence there is a lack of a minimizer belonging to an "appropriate" underlying Sobolev space, in general. Instead, corresponding (weakly converging) minimizing sequences are studied that typically show fast oscillations in the gradient of the deformation which gives raise to microstructure. A tool for describing the asymptotic behavior of minimizing sequences is the Young measure [21], giving volume fractions of the involved martensitic variants in each test volume of the reference domain in austenite state Ω. This probability measure enables the evaluation of (nonlinear) quantities, like the stress for the limit of such minimizing sequences [21].

From the numerical point of view, the computation of minimizers associated with discrete models leads to significant problems, mainly caused by their non-convex character. Over the last years, basically three categories of methods have been studied to cope with this type of problem:

[1]Department of Mathematics and Statistics, University of Maryland, Baltimore County, 1000 Hilltop Circle, Baltimore, MD 21250, U.S.A. (gobbert@math.umbc.edu).

[2]Mathematisches Seminar, Christian-Albrechts-Universität Kiel, Ludewig-Meyn-Str. 4, D–24098 Kiel, Germany (apr@numerik.uni-kiel.de).

1. *Convexification of the energy functional*, see, e.g., [4, 10, 14, 21]: The original non-convex elastic energy density is replaced by its (quasi- or rank-one-)convex hull. This manipulation is attractive since now a minimizer exists that is the weak limit of a minimizing sequence. Equally important, the solution of this problem is now accessible to standard conjugate gradient type minimization routines. On the other hand, explicit formulae of (quasi-)convex hulls are only known in some cases (unfortunately, the physically important case of the Ericksen-James energy functional is not covered, yet), and numerical approximations of it are rather expensive, see [4, 14]. Moreover, this process deletes physical information from the original energy functional that makes this approach questionable for certain important applications.

2. *Generalized formulation of the energy functional*, see, e.g., [5, 21, 23]: The original problem is reformulated as a convex minimization problem in terms of the deformation and parameterized gradient Young measures. This approach is quite promising from a theoretical point of view since the energy functional is kept unchanged. As a drawback, it causes significant computational work which necessitates additional sophisticated numerical strategies. A first promising step to reduce computational work is given in [5], where a one-dimensional test problem is studied.

3. *Direct minimization of the energy functional*, see, e.g., [8, 11, 15, 16, 18, 19]: Numerical methods that fit into this category start with discretizations of the energy functional and underlying domain via e.g., finite element methods. These methods preserve the physical energy density and are applicable without restrictions. On the other hand, they might suffer severely from the non-convex character of the energy density in that computed minimizers often get stuck in local minima. Furthermore, the spatial discretization introduces a scaling to the microstructure that limits the resolution of complex microstructure. At the same time, this drawback of local minima is sometimes advantageous for applications where local minima (e.g., "metastable states") are important (e.g., in hysteresis phenomena).

In the following, we consider finite element methods that are intended for the direct minimization of non-convex functionals. In the context of the Ericksen-James energy density, we refer to the extensive survey article by Luskin [19] and the publications [15, 16, 18] that deal with the numerical analysis of conforming and classical non-conforming methods (i.e., continuity is only enforced in the center of adjacent finite element faces). As is pointed out in these contributions, the resolution of microscale structures heavily relies on the alignment of the underlying mesh with the laminated microstructure, otherwise leading to drastically polluted solutions.

This is the basic motivation for the introduction of discontinuous finite element methods to this type of minimization problem. As is can be clearly seen from the theoretical investigations performed in [11], the convergence analysis leads to results that are superior to those of conforming and classical non-conforming methods, which reflects the increased flexibility of the finite element method with respect to the underlying triangulation; see Table 1 for a comparison of the methods discussed here.

As shown in [22], we can further increase accuracy of the discontinuous finite element method by adding an 'adaptive component,' together with a mesh-refinement strategy that is based on large inter-element jumps.

The goal of this paper is the continuation of our comparison of distinct finite element methods in the contents of non-convex minimization by presenting thorough computational test studies. We stress the fact that the computational results that are presented for a prototype energy density (for deformations $u : \mathrm{R}^2 \supset \Omega \to \mathrm{R}$) here are superior to most of the theoretical ones listed in Table 1 and Theorem 1, which is due to dimensionality arguments needed in the analysis for the Ericksen-James energy dealing with deformations $u : \mathrm{R}^3 \supset \Omega \to \mathrm{R}^3$.

The outline of the paper is as follows: Section 2 gives a short summary of the Ericksen-James energy functional dealing with admissible three-dimensional deformations, and states the main theorem quoted from [11]. Section 3 proceeds with the presentation of a thorough case study for a prototype problem for simple laminates originally proposed by Bolza, see, e.g., [21]. A study for a more complex example due to Tartar is addressed in Section 4 to show the general applicability of the presented discontinuous finite element method.

2 The Ericksen-James energy. Mathematical models for describing deformations from a reference state of "smart materials" can be formulated in two or three dimensions, i.e., $d \in \{2, 3\}$. The numerical problem reads then as follows. For the reference state $\Omega \in \mathrm{R}^d$, minimize the energy functional

$$\mathcal{E}(v) = \int_\Omega \phi(\nabla v(x))\, d\Omega \tag{1}$$

over all admissible functions $v \in \mathcal{A}$ with

$$\mathcal{A} = \left\{ u \in C(\bar{\Omega}; \mathrm{R}^d) : u|_{\partial\Omega} = g(x) \right\}. \tag{2}$$

Here, $\phi : \mathrm{R}^{d\times d} \to \mathrm{R}$ is the Ericksen-James energy that only depends on the gradient ∇v of the deformation v [1, 2], and $g(x)$ is a given function on the boundary of Ω.

For coefficients b, c, d, e, f of the material under consideration, that are fixed by experimental data, the multi-well Ericksen-James energy density can be written in the following form, see [13, 19],

$$\begin{aligned}
\phi(A) = {} & \frac{b}{6}\left[\left(\frac{3A_{11}}{\mathrm{tr}A} - 1\right)^2 + \left(\frac{3A_{22}}{\mathrm{tr}A} - 1\right)^2 + \left(\frac{3A_{33}}{\mathrm{tr}A} - 1\right)^2\right] \\
& + \frac{c}{2}\left(\frac{3A_{11}}{\mathrm{tr}A} - 1\right)\left(\frac{3A_{22}}{\mathrm{tr}A} - 1\right)\left(\frac{3A_{33}}{\mathrm{tr}A} - 1\right) \\
& + \frac{d}{36}\left[\left(\frac{3A_{11}}{\mathrm{tr}A} - 1\right)^2 + \left(\frac{3A_{22}}{\mathrm{tr}A} - 1\right)^2 + \left(\frac{3A_{33}}{\mathrm{tr}A} - 1\right)^2\right]^2 \\
& + e\left(A_{12}^2 + A_{13}^2 + A_{23}^2 + A_{21}^2 + A_{31}^2 + A_{32}^2\right) + f\left(\mathrm{tr}A - 3\right)^2,
\end{aligned} \tag{3}$$

where $A = F^T F$ is the right Cauchy-Green strain and $\mathrm{tr}A$ the trace of A. The elastic energy density satisfies the principle of frame indifference which necessarily leads to a non-convex

function. For a detailed discussion on the physical background of the energy, we refer to, e.g., [19]. For the subsequent studies, we benefit from the density $\phi(\cdot)$ being non-negative and $\phi(A) = 0$ if and only if $A \in \mathcal{U}$, where $\mathcal{U}$ denotes the union of all energy wells. These wells correspond to symmetry-related energy-minimizing states of the material.

In order to have minimizers being Lipschitz-continuous, the wells have to be rank-one connected. For the case of a two-well problem, this implies the condition

$$\exists\, F_i \in \mathcal{U}_i,\ i = 1, 2 \qquad \exists\, a, n \in \mathrm{R}^3 \qquad \text{s.t.} \qquad F_2 = F_1 + a \otimes n.$$

Here, $\otimes$ denotes the tensor product of the vectors a and n, that is, $(a \otimes n)_{ij} = a_i n_j$. Without loss of generality, we may assume $|n| = 1$ for the vector n pointing in the direction perpendicular to the laminates. For the sake of uniqueness of the Young measure that is associated with the microstructure [1, 2], we prescribe affine boundary conditions

$$u(x) = F_\lambda x \quad \text{for } x \in \partial\Omega \tag{4}$$

with

$$F_\lambda = \lambda F_1 + (1 - \lambda) F_2 \tag{5}$$

with volume fraction $\lambda \in [0, 1]$. These characterizations of admissible deformations generalize to the multiple well case of several energetically equivalent crystallographic configurations, see, e.g., [19].

The first finite element methods for the minimization of (1) used conforming elements with piecewise linear basis functions on each triangular or quadrilateral element, thus minimizing on a set of admissible functions $\mathcal{A}_h \subset \mathcal{A}$. For *convex* energy densities ϕ, this approach is known to yield optimal convergence results for the energy with order $\mathcal{O}(h^2)$. However, for problem (3) with a non-convex energy density, it can only be shown that a minimizing deformation $u_h \in \mathcal{A}_h$ satisfies

$$\mathcal{E}(u_h) \leq C h^{1/2}, \tag{6}$$

where the constant C may depend on the coefficients of the problem, the triangulation $\mathcal{T}_h$ and the domain Ω, but not on the mesh parameter h, see [6, 8, 16, 18, 19]. Moreover, it turns out that the quality of the approximation depends strongly on the degree of alignment of the numerical mesh with the physical laminates. This means that the laminate microstructure is well-resolved on meshes, whose element edges run along the laminate direction. If this is not the case, the numerical results are often significantly polluted so that the laminates are distorted beyond recognition; see Figure 2 for an example, which will be discussed in detail in Section 3.

The sharpness of these suboptimal convergence results has been investigated by Chipot and Müller [7] for a different, non-convex energy density and related deformations $u : \Omega \to \mathrm{R}$ with $\Omega \subset \mathrm{R}^2$. In particular, they verified the existence of triangulations $\mathcal{T}_h$ of the domain Ω such that the energy of a minimizer $u_h \in \mathcal{A}_h$ is at least $\mathcal{O}(h^{2/3})$.

As a second numerical approach, a classical non-conforming finite element method with continuity only in the edge midpoints (the Crouzeix-Raviart element) has been used [9, 12,

19]; even more general three dimensional non-conforming elements have been used in [13] and analyzed in [15]. This method relaxes the continuity constraints between each two elements by only requiring continuity of the discrete deformations at the edge midpoints. Of course, the functional $\mathcal{E}(\cdot)$ is then defined in an appropriate element-wise setting by taking $\mathcal{E}_h(\cdot)$. This finite element method does have increased flexibility to handle deformations with microstructure on general grids due to the relaxation of the inter-element continuity requirements. However, the theoretical analysis presented in [12, 15] does not reflect this improved flexibility in comparison to the conforming method, and the result for a minimizer $u_h \in \mathcal{A}_h$ is still

$$\mathcal{E}_h(u_h) \leq Ch^{1/2}. \tag{7}$$

This motivates the construction of a new finite element method yielding more accurate approximations of crucial quantities such as the macroscopic deformation, the structure of laminates, and the statistical properties of the microstructure given in terms of its Young measure on non-aligned meshes. Moreover, this new method should be able to represent more complex microstructure given through force-driven deformations as well as ones occurring in evolutionary models both in this context and for more complicated materials.

A new algorithm based on discontinuous finite elements was introduced in [11]. As it is shown there, this algorithm allows for much improved convergence rate estimates for the energy (namely $\mathcal{O}(h^2)$ for the energy of a minimizing deformation) as well as other quantities of interest like the Young measure or the deformation gradient in laminate direction. In particular, this result holds for non-aligned meshes, i.e., those that are independent of the alignment of the numerical grid with the physical laminates. The underlying conceptual ideas are the following:

1. The (averaged) boundary conditions will be treated in a more relaxed way to avoid the pollution impact from the boundary.
2. The cross-element continuity constraints are relaxed in the sense that small jumps are allowed.
3. The laminate structures are scaled differently from the transitions between laminates.

This leads to the following algorithm:

Algorithm 1 *Given a quasiuniform triangulation $\mathcal{T}_h$ of the domain $\Omega \subset \mathrm{R}^d$, with $d \in \{2,3\}$, consider element-wise linear deformations $v_h \in \mathcal{A}_h \equiv \prod_{K\in\mathcal{T}_h} \mathcal{P}_1(K)$ with the scaled energy functional*

$$\begin{aligned}\mathcal{E}_h^\beta(v_h) = &\sum_{K\in\mathcal{T}_h} \int_K \phi(\nabla v_h(x))\, d\Omega \\ &+ \alpha_{11}\Big(\sum_{K\in\mathcal{T}_h} h^{1-\beta} \int_{\partial K} \big|[v_h](x)\big|\, d\sigma\Big)^2 + \alpha_{12}\Big(\sum_{K\in\mathcal{T}_h} h^{1-\beta} \int_{\partial K} \big|[v_h](x)\big|^2\, d\sigma\Big) \\ &+ \alpha_2 \sum_{K\in\mathcal{T}_h} h^{2\beta} \int_{\partial K\cap\partial\Omega} |v_h(x) - g(x)|^2\, d\sigma + \alpha_3 \sum_{K\in\mathcal{T}_h} h^{2\beta} \int_K |v_h(x) - g(x)|^2\, d\Omega,\end{aligned} \tag{8}$$

with $g(x) = F_\lambda x$, and perform the minimization

$$\min_{v_h \in \mathcal{A}_h} \mathcal{E}_h^\beta(v_h) \tag{9}$$

for a fixed constant $\beta \in [0,1]$.

The coefficients $\alpha_{11}, \alpha_{12}, \alpha_2, \alpha_3$ are order one constants that control the relative contributions from the inter-element continuity constraints, the relaxation of the boundary condition, and the approximation of the macroscopic deformation. As it turns out, an algorithm appropriate for representing laminate microstructure on non-aligned meshes has to incorporate the third feature in the list above in that it should be able to distinguish between contributions to a minimizer from the laminate microstructure and from the transitions between laminates. Therefore, Algorithm 1 introduces a different scaling of laminates (which are of order $\mathcal{O}(h^{1-\beta})$) and of transitions between laminates (of order $\mathcal{O}(h)$).

We distinguish between two versions of the scaled energy functional $\mathcal{E}_h^\beta(\cdot)$ by setting either $\alpha_3 = 0$ or $\alpha_3 \neq 0$. For both versions of the discontinuous element method, an energy estimate of $\mathcal{O}(h^2)$ holds [11]. This is optimal for the linear basis functions in use. However, also other quantities are important for practical purposes: The first version (i.e., $\alpha_3 = 0$) cancels out the contribution from the L^2-norm of the deformation on the interior finite elements and gives rise to an energy density that is rotationally invariant, whereas the second one (i.e., $\alpha_3 \neq 0$) is not rotationally invariant anymore, but allows for better approximation of, in particular, the deformation gradient ∇u_h in laminate direction $w \in \mathrm{R}^3$ and of the local volume fraction λ^i of the i-th variant of the martensitic phase in a subdomain $\omega \subset \Omega$. More precisely, the volume fractions $\mu(\omega_\rho^i(u_h))/\mu(\omega)$ give approximations to the λ^i, $i \in \{1,2\}$, with $\mu(\omega)$ the measure of the subdomain ω and $\mu(\omega_\rho^i(u_h))$ the measure of that collection of elements $\omega_\rho^i \subset \omega$, on which the deformation gradient ∇u_h is inside a ball with radius ρ and center F_i (measured in the Frobenius norm). These quantities are crucial parameters in the computation of the Young measure generated by the deformation gradient ∇u_h [4]. As already stated, the Young measure in turn yields important macroscopic quantities of practical relevance, for instance, the stress field, see [4, 19] and the literature cited therein. It is for this reason that the accurate approximation also of microscopic quantities like the deformation gradient and volume fraction is of importance. For the sake of completeness, we recall here the main theorem that is verified in [11]. For further explanation of notation used, we refer the reader to the remainder of this section.

Theorem 1 *Consider problem (9), with $\beta = 1/2$, as an approximation of the minimization problem (1)–(2) with $\Omega \subset \mathrm{R}^3$ a bounded set, and suppose $u \in \mathcal{A}$ is a weak limit solution of problem (1)–(2) yielding zero energy. Then problem (9) has at least one solution $u_h \in \mathcal{A}_h \equiv \prod_{K \in \mathcal{T}_h} \mathcal{P}_1(K)$, and u_h satisfies the following convergence estimates, for all $\omega \subset \Omega$ and $h < \rho < 1$, and all $\rho > 0$,*

1. *(Case $\alpha_3 = 0$) for positive constants $\alpha_{11}, \alpha_{12}, \alpha_2 = \mathcal{O}(1)$ and $\alpha_3 = 0$*

   (a) $\mathcal{E}_h^{1/2}(u_h) \leq Ch^2$,

   (b) $\|u_h - F_\lambda x\|_{L^2(\Omega)} \leq Ch^{1/4}$,

Finite element method	$\mathcal{E}_h(u_h)$	$\|u_h - F_\lambda x\|$	$\|(\nabla u_h - F_\lambda)\, w\|$	$\left\|\frac{\mu(\omega_\rho^i(u_h))}{\mu(\omega)} - \lambda^i\right\|$
conforming [18, 19]	$\mathcal{O}(h^{1/2})$	$\mathcal{O}(h^{1/8})$	$\mathcal{O}(h^{1/8})$	$\mathcal{O}(h^{1/16})$
classical non-conforming [15]	$\mathcal{O}(h^{1/2})$	$\mathcal{O}(h^{1/8})$	$\mathcal{O}(h^{1/8})$	$\mathcal{O}(h^{1/16})$
discontinuous without interior L^2-term ($\alpha_3 = 0$) [11]	$\mathcal{O}(h^2)$	$\mathcal{O}(h^{1/4})$	$\mathcal{O}(h^{1/4})$	$\mathcal{O}(h^{1/8})$
discontinuous with interior L^2-term ($\alpha_3 \neq 0$) [11]	$\mathcal{O}(h^2)$	$\mathcal{O}(h^{1/2})$	$\mathcal{O}(h^{1/4})$	$\mathcal{O}(h^{1/4})$

Table 1: Summary of convergence results for the energy and other crucial quantities for different finite element methods.

(c) $\|(\nabla u_h - F_\lambda)w\|_{L^2(\Omega)} \leq Ch^{1/4}$,

(d) $\left|\frac{\mu(\omega_\rho^i(u_h))}{\mu(\omega)} - \lambda^i\right| \leq Ch^{1/8}$, *for* $i \in \{1,2\}$,

2. *(Case* $\alpha_3 \neq 0$*) for positive constants* $\alpha_{11}, \alpha_{12}, \alpha_2, \alpha_3 = \mathcal{O}(1)$

(a) $\mathcal{E}_h^{1/2}(u_h) \leq Ch^2$,

(b) $\|u_h - F_\lambda x\|_{L^2(\Omega)} \leq Ch^{1/2}$,

(c) $\|(\nabla u_h - F_\lambda)w\|_{L^2(\Omega)} \leq Ch^{1/4}$,

(d) $\left|\frac{\mu(\omega_\rho^i(u_h))}{\mu(\omega)} - \lambda^i\right| \leq Ch^{1/4}$, *for* $i \in \{1,2\}$.

The generic constant C may depend on the parameters of the continuous minimization problem, with energy (1) and the values $\alpha_{11}, \alpha_{12}, \alpha_2, and \alpha_3$, but not on the mesh parameter h. In the cases (d), it additionally depends on the choice of ρ.

The analytic convergence results for all quantities of interest and the different finite element methods that are subject to computational comparison in the following are summarized in Table 1. Here, $\|\cdot\|$ stands for the L^2-norm. Moreover, the constants λ^i, $i \in \{1,2\}$, denote the coefficients of the Young measure that are approximated by the volume fraction $\mu(\omega_\rho^i(u_h))/\mu(\omega)$; for the double well problem, this is concretely $\lambda^1 = \lambda$ and $\lambda^2 = 1 - \lambda$ in our double-well case. A marked improvement over the classical methods can be observed for all quantities.

3 A case study for simple laminates.

3.1 The prototype problem. In order to demonstrate the theoretical results of the previous sections numerically, we consider the following prototype problem for the Ericksen-

James energy [4, 10]

$$\mathcal{E}(v) = \int_\Omega \left((v_x)^2 - 1\right)^2 + (v_y)^2 \, d\Omega \tag{10}$$

for the domain $\Omega = (0,1) \times (0,1) \subset \mathrm{R}^2$ and the deformations $v : \Omega \to \mathrm{R}$ with boundary condition $v = 0$ on $\partial\Omega$. This problem possesses crucial features of the full problem involving (3) in two or three dimensions. The solution to this problem consists of laminates in the y-direction, because the stress-free deformation gradients $\nabla v = (v_x, v_y)$ are $F_1 = (+1, 0)$ and $F_2 = (-1, 0)$.

In order to study the dependence of the finite element method on the alignment of the numerical mesh with the physical laminates, we consider the following generalized energy functional

$$\mathcal{E}(v) = \int_\Omega \left((\nabla v \cdot n)^2 - 1\right)^2 + (\nabla v \cdot w)^2 \, d\Omega. \tag{11}$$

Here, $n = n(\gamma) = (\cos(\gamma), \sin(\gamma))^T$ denotes the vector normal to the laminate direction, $w = w(\gamma) \in \mathrm{R}^2$ is a vector along the laminates and orthogonal to n, and γ the angle between the positive x-axis and the vector n, see Figure 1. For $\gamma = 0°$, the generalized energy in (11) reduces to the one in the original problem (10). Since the prototype problem with boundary condition $u = 0$ on $\partial\Omega$ models the example of simple laminates, the coefficients of the Young measure λ^1 and λ^2 have to equal $1/2$ in all cases.

The simulations presented in this paper have been performed for three different finite elements: conforming, classical non-conforming, and discontinuous finite elements. We set $\beta = 0$ and $\alpha_{11} = \alpha_{12} = \alpha_3 = 0$ for both the conforming and the classical non-conforming elements in order for the generalized energy functional in Algorithm 1 to recover the original energy functional, namely

$$\mathcal{E}_h^0(v_h) = \sum_{K \in \mathcal{T}_h} \int_K \phi(\nabla v_h(x)) \, d\Omega + \alpha_2 \sum_{K \in \mathcal{T}_h} \int_{\partial K \cap \partial\Omega} |v_h(x) - F_\lambda x|^2 \, d\sigma \tag{12}$$

with the boundary conditions implemented via a penalty approach. For the discontinuous element, the coefficient β is set to $1/2$, since this is the optimal choice, according to the analysis performed in [11].

The angle γ is varied through five values, that cover all degrees of alignment of the physical laminates with the numerical mesh, namely $\gamma \in \{-45°, -22.5°, 0°, +22.5°, +45°\}$. The numerical grid is given by a regularly refined triangular mesh independent of the angle γ and such that the mesh is fully aligned with the physical laminates when $\gamma = -45°$. To determine the convergence rate for the energy, the mesh parameter was chosen as $h \in \{\frac{1}{4}, \frac{1}{8}, \frac{1}{16}, \frac{1}{32}, \frac{1}{64}\}$. In all cases, the simulations were performed up to relative tolerances of 10^{-3} and 10^{-4} in the energy in two consecutive iterations. A study for the parameter α_2 governing the degree of relaxation of the boundary term was performed. It was varied through the values $\alpha_2 \in \{0.1, 1, 10, 100, 1000, 10000\}$ for the classical elements and $\alpha_2 \in \{1, 1000\}$ for the discontinuous element. For the discontinuous element, results using $\alpha_3 = 0$ and $\alpha_3 = 1$ were compared. For convenience, Table 2 summarizes the problem parameters used for the tables

Label	finite element	boundary conditions	β	α_{11}	α_{12}	α_2	α_3
(a)	conforming	exact	0	0	0	1000	0
(b)	conforming	relaxed	0	0	0	1	0
(c)	classical non-conforming	exact	0	0	0	1000	0
(d)	classical non-conforming	relaxed	0	0	0	1	0
(e)	discontinuous	relaxed	1/2	1	1	1	0

Table 2: Values of the coefficients in the energy functional for the tables in Section 3.

below.

The energy functional of Algorithm 1 is discretized using the package FEAT2D [3] for the underlying finite element discretization. New element routines were defined in this package for the discontinuous finite element for our purposes. The computer program implements the nonlinear conjugate gradient method for the minimization with a quadratic fit line search after bracketing [17].

For the graphs presented in the following, the angle $\gamma = +22.5°$ is chosen, since it is the "least" aligned case between the laminates and the grid. It is known that this case poses significant problems for the classical finite element discretizations; for instance, figures for conforming finite elements in [19] exhibit 'polluted' laminates, whose direction is not correct and for which the volume fraction $\mu(\omega^i_\rho(u_h))/\mu(\omega)$ is not correct for subdomains $\omega \subset \Omega$. The corresponding figure in this paper is Figure 2, see below.

3.2 The conforming finite element. Figure 2 shows numerical results obtained for the conforming finite element. This element has been considered by Collins, see [8, 9], and the convergence analyses are contained in [6, 16, 18, 19]. Figure 2 (a) shows a color-coded graph of the deformation gradient ∇u_h in normal direction n (with $\rho = 0.1$). The laminates do not follow their correct direction of $\gamma = +22.5°$ anymore, but are rather distorted, and no reliable information concerning the volume fractions can be obtained. Figure 2 (b) shows the deformation u_h confirming the observations. (This larger size for h was chosen in Figure 2 (b) to allow the laminates to be visible, but the results have been observed for all values of h.)

This observation is verified by the values of the energy functional for the conforming finite element method in Table 4 (a). We notice that for $\gamma = -45°$ and $\gamma = 0°$ the convergence rate is linear. This is explained by the fact that in these two cases the numerical mesh is aligned with the direction of the physical laminates. In the general case however, as seen in the remaining columns of the table including the one for $\gamma = +22.5°$, the convergence rate is observed to be much less than $\mathcal{O}(h)$ in general.

Tables 5 (a), 6 (a), and 7 (a) show the numerical results for the quantities listed in columns 2, 3, and 4 of Table 1 above. For the L^2-error of the deformation in Table 5 (a), we observe nearly linear convergence for all angles γ, which is significantly better than the theoretical convergence rate of $\mathcal{O}(h^{1/8})$, see Table 1. However, the L^2-error of the deformation gradient in laminate direction in Table 6 (a) depends on the alignment of the numerical mesh. Even more apparent is this dependence for the error in the approximation of the volume fraction λ^1 in Table 7 (a), even though the convergence rate is better than predicted theoretically, again.

The 'exact' boundary conditions above are achieved by setting the penalty parameter $\alpha_2 = 1000$ in the algorithm. The penaltization technique is seen to work effectively and efficiently, and the contribution from the boundary to the total energy is (much) less than 10 %. That is, practically all error in the conforming finite element method with exact boundary conditions results from the bulk term in the energy functional. This motivates the relaxation of the enforcement of the boundary conditions by choosing smaller values for α_2. The results for the conforming method with 'relaxed' boundary conditions are listed in Tables 4 (b), 5 (b), 6 (b), and 7 (b). In the aligned cases for $\gamma = -45°$ and $0°$, the contribution from the bulk energy is now nearly vanishing, showing the effect of freeing the discretization from satisfying the (averaged) boundary conditions. The convergence rates in these cases is improved to nearly $\mathcal{O}(h^2)$ for the energy, which is dominated by residual error from the boundary. This behavior is also well-understood from the analytical point of view, since interpolation errors on the actual triangulation and approximation errors due to prescribed averaged solution data compete in the minimization process, see [6, 18]. However, for the non-aligned meshes, the size of the interpolation error has not improved. This demonstrates that the numerical mesh itself is responsible for the poor quality of the approximation in general. The error of the deformation in Table 5 (b) shows the same behavior as before. Both Tables 6 (b) and 7 (b) for quantities describing the laminated microstructure show a marked improvement in the aligned cases, but none in the general non-aligned cases. Therefore, relaxing the enforcement of the boundary conditions is not sufficient for obtaining reliable approximations to the Young measure, when using conforming finite elements.

For the ranges of the mesh size h used in this study, the boundary conditions are not even satisfied in an averaged sense anymore if $\alpha_2 \leq 0.1$, while for $\alpha_2 \geq 10000$, the laminate structure in the interior of the domain is not resolved anymore. We close with the observation that the number of iterations needed to achieve a certain tolerance depends naturally on the angle γ and the tolerance requested, but improves with a relaxed implementation of the boundary conditions when lowering α_2.

3.3 The classical non-conforming finite element. As an example for classical non-conforming elements, we used the Crouzeix-Raviart element, for which the edge midpoints are the degrees of freedom. Continuity from element to element is not enforced along the element edges, but only at the edge midpoints. This element has been proposed for the simulation of microstructures in [9] and analyzed in [12, 15]. The fundamental idea is to increase the flexibility of the finite element approximation in order to adjust better to the direction of the laminates and hence to decrease the interpolation error measured by the bulk term of the energy.

It can be seen both in Figures 3 (a) and (b) that there is a significant improvement over Figure 2 in that the computed laminates run in the correct direction given by the angle $\gamma = +22.5°$, and the laminate transitions are represented crisply.

Table 4 (c) shows the energy values obtained for the classical non-conforming element. We observe that the values are improved over the corresponding conforming ones, but not the convergence rates. Tables 5 (c), 6 (c), and 7 (c) show some improvement over the conforming elements, in particular in the mildly misaligned case of $\gamma = -22.5$. However, in the severely misaligned case of $\gamma = +22.5$, no improvement is observable. Moreover, it is observed that

the bulk term of the energy still accounts for more than 90 % of the energy, that is the mesh pollution effect on the minimizer is still present.

As in the conforming case, the enforcement of the boundary conditions in the penalty formulation is now relaxed by decreasing the value of α_2. As Tables 4 (d), 5 (d), 6 (d), and 7 (d) show, any improvements are concentrated on the aligned cases of angles $\gamma = -45°$ and $\gamma = 0°$, as for the conforming element. In those cases, the total energy is now made up of error from the boundary, while in the remaining cases, the energy still results from the bulk term to at least 90 %. It has to be concluded that the classical non-conforming element possesses more flexibility to represent the laminates (see the figures), but it does not decrease the interpolation error independently of the mesh alignment (see the tables), thus validating the theoretical result (7) in general.

3.4 The discontinuous finite element. Figure 4 reports the results for the discontinuous element. This element uses the vertices as degrees of freedom without any continuity requirement in the definition of the finite element; the amount of discontinuity allowed is controlled via a penalty technique implemented by the α_{11}- and α_{12}-terms in the energy function in Algorithm 1. The discontinuous element was originally introduced and analyzed theoretically in [11].

It is observed in Figure 4 (a) that the bands of the laminates are represented crisply and running straight and in the correct direction. The laminates themselves are wider than in the classical cases; this coincides with the theoretical investigation in [11] that deformations with laminate widths of $\mathcal{O}(h^{1-\beta})$ (with $\beta = 1/2$) are favored. In Figure 4 (b), we see that the solution exhibits a certain degree of discontinuity in the interior, as expected, but this effect is limited to the element edges that make up the transitions from one laminate to another, while the laminates themselves are represented continuously.

Table 4 (e) lists the values of the energy for the discontinuous element. We can observe nearly quadratic convergence rates in most entries, which is clearly independent of the alignment of the numerical mesh with the physical laminates. This independence is confirmed throughout the tables. In particular, Tables 5 (e) and 6 (e) exhibit slightly better convergence rates than predicted in Table 1. On the one hand, the absolute values for the error in the deformation in Table 5 (e) are slightly higher than for the previous elements due to the wider laminates. On the other hand, the values for the error in the deformation gradient in laminate direction in Table 6 (e) are significantly smaller than before, indicating the crisper representation of the microscopic laminates. Finally, Table 7 (e) shows that the volume fraction $\mu(\omega_\rho^i(u_h))/\mu(\omega)$ is computed without error in many instances. Notice that for the previous elements, this behavior occurred only in the aligned cases.

The above refers to the discontinuous element using $\alpha_3 = 0$; exactly the same observations hold for the discontinuous element with $\alpha_3 = 1$. For our approach using a discontinuous finite element, the enforcement of the boundary conditions is usually relaxed by choosing $\alpha_2 = 1$, see Section 1. When α_2 is increased to 1000, only the solution on the elements with nodes on the boundary changes, since the construction allows for inter-element discontinuity. Also in this case, all convergence results continue to hold independent of α_2. Indeed, the absolute values of the total energy turn out to depend on α_2 (the degree of relaxation of the boundary condition), but not on the angle γ (the mesh alignment), the coefficient α_3 (the interior L^2-

term), or the requested tolerance. Generally, the total energy is smaller on the aligned grids than in the non-aligned cases. The contribution from the boundary error is comparable in absolute values in all cases. The difference in the energy between aligned and non-aligned cases is made up nearly solely by contributions from the jump terms with coefficients α_{11} and α_{12}, which are very small in the aligned cases. However, if the resolution is sufficiently good ($h \leq 1/32$), the bulk term in the energy functional contributes at most 5 % to the total energy. This demonstrates that the discontinuous finite element method is capable of resolving the simple laminate structure independent of the mesh alignment, since the interpolation error is uniformly small.

The number of iterations needed to achieve a certain tolerance depends naturally on the tolerance, but only weakly on the enforcement of the boundary conditions (α_2) and the mesh alignment (γ); the number of iterations did not depend on the coefficient α_3.

4 The example by Tartar. This section shows the increased flexibility of the discontinuous finite element method in another test example due to Tartar, see [20] involving a more complicated microstructure. Numerical studies on this problem for convexified energies or generalized formulations have been performed in [20] and [4], respectively.

We consider the minimization of the following energy, for $\Omega = (0,1) \times (0,1)$,

$$\tilde{\mathcal{E}}(v) = \int_\Omega \left(v_x^2 - 1\right)^2 + v_y^2 \, d\Omega + \int_\Omega \left[-\tfrac{3}{128}\left(x - \tfrac{1}{2}\right)^5 - \tfrac{1}{3}\left(x - \tfrac{1}{2}\right)^3 - v\right]^2 d\Omega. \tag{13}$$

As is known from Tartar's one dimensional example, the minimum of the relaxed problem is given by

$$u(x,y) = \begin{cases} -\tfrac{3}{128}\left(x - \tfrac{1}{2}\right)^5 - \tfrac{1}{3}\left(x - \tfrac{1}{2}\right)^3 & \text{for } 0 \leq x \leq \tfrac{1}{2} \\ \tfrac{1}{24}\left(x - \tfrac{1}{2}\right)^3 + \left(x - \tfrac{1}{2}\right) & \text{for } \tfrac{1}{2} < x \leq 1. \end{cases} \tag{14}$$

The minimum energy [21] is given by a positive value, i.e., $\inf_{v \in \tilde{\mathcal{A}}} \tilde{\mathcal{E}}(v) = \frac{1409}{30000}$, for $\tilde{\mathcal{A}} = \left\{v \in W_g^{1,4}(\Omega), g = u\big|_{\partial\Omega}\right\}$, and minimizing sequences exhibit spatial oscillations, i.e., microstructure, on the domain $\Omega_m = (0, \frac{1}{2}) \times (0,1)$.

The conforming and the discontinuous finite element methods were applied to this problem in order to clarify the impact of general triangulations and given boundary data on computed minimizers. To this end, the energy functional (13) is 'rotated' in the way as in (11) for the energy functional in (10). A rotation by $\gamma = +22.5°$ is presented here. The results are presented in the Figures 5 and 6 for the conforming and the discontinuous element, respectively. As can be clearly seen again, there is significant pollution of the laminate microstructure on parts of the domain for the conforming method in Figure 5. The discontinuous method produces the minimizers in Figure 6 with crisp laminates in the appropriate part of the domain.

Table 3 lists the values for the energy functional obtained for both finite elements methods. Clearly, the discontinuous method attains significantly lower values, but they stabilize above 0 in both cases, as expected for this problem, although the minimum energy in the 'rotated' case is not given explicitly. Moreover, it is observed that the contribution from the second integral in (13) above is comparable in absolute terms for both methods; the main

Finite element	conforming	discontinuous
$h = 1/4$	0.4263	0.1387
$h = 1/8$	0.3468	0.0696
$h = 1/16$	0.2480	0.0492
$h = 1/32$	0.1938	0.0360
$h = 1/64$	0.1674	0.0309

Table 3: Total energy for the Tartar example for the conforming and the discontinuous element.

contributor to the larger energy with at least 80 % for the conforming method is the first integral. This again reflects the dependence of the minimizer on the underlying numerical mesh for the conforming finite element and the increased flexibility of the method using the discontinuous finite element.

5 Conclusions. Results for an extensive case study for prototype problems for the simulation of crystalline microstructure have been presented for three finite elements: conforming, classical non-conforming, and discontinuous finite elements. The quality of both the conforming and the classical non-conforming elements are seen to depend on the alignment of the numerical grid with the physical laminates, with decreasing quality on general triangulations, as demonstrated by the results of the case study in Section 3. Also, relaxation of the enforcement of the boundary conditions in the case of the classical elements did not improve their convergence behavior, in general. In contrast, the results for the discontinuous element show optimal convergence behavior on general meshes, independent of the mesh alignment. All three elements studied in this paper represent the macroscopic deformation quite well, but only the discontinuous element represents the crucial microscopic quantities like the deformation gradient in laminate direction and the coefficient of the corresponding Young measure adequately. Also for the more complex microstructure in Section 4, the discontinuous element shows good performance compared to the classical elements. This demonstrates the superiority of the discretization using discontinuous finite elements for practical applications. These computational results are in agreement with analytic results contained in [11].

Acknowledgments. The authors would like to thank the Institute for Mathematics and its Applications at the University of Minnesota for the stimulating environment during our stay as well as for the use of its computer facilities, on which the numerical code was developed.

	$\gamma = -45°$	$\gamma = -22.5°$	$\gamma = 0°$	$\gamma = +22.5°$	$\gamma = +45°$
$h = 1/4$	0.5754	0.5305	0.4532	0.6690	0.8920
$h = 1/8$	0.3497	0.3604	0.3891	0.4617	0.6182
$h = 1/16$	0.1884	0.2634	0.1939	0.3444	0.4260
$h = 1/32$	0.0972	0.1958	0.0963	0.2512	0.2911
$h = 1/64$	0.0488	0.1587	0.0474	0.1956	0.2320

(a)

	$\gamma = -45°$	$\gamma = -22.5°$	$\gamma = 0°$	$\gamma = +22.5°$	$\gamma = +45°$
$h = 1/4$	0.1703	0.2791	0.1145	0.2460	0.5335
$h = 1/8$	0.0435	0.1563	0.0425	0.2510	0.3300
$h = 1/16$	0.0113	0.1251	0.0112	0.1676	0.3227
$h = 1/32$	0.0029	0.1180	0.0029	0.1659	0.3459
$h = 1/64$	0.0007	0.1162	0.0007	0.1861	0.3758

(b)

	$\gamma = -45°$	$\gamma = -22.5°$	$\gamma = 0°$	$\gamma = +22.5°$	$\gamma = +45°$
$h = 1/4$	0.2297	0.2629	0.3733	0.3833	0.3265
$h = 1/8$	0.1532	0.1744	0.1996	0.2315	0.2200
$h = 1/16$	0.0885	0.0980	0.0992	0.1438	0.1507
$h = 1/32$	0.0470	0.0652	0.0491	0.0960	0.1085
$h = 1/64$	0.0238	0.0392	0.0243	0.0765	0.0679

(c)

	$\gamma = -45°$	$\gamma = -22.5°$	$\gamma = 0°$	$\gamma = +22.5°$	$\gamma = +45°$
$h = 1/4$	0.1422	0.1982	0.0880	0.2305	0.0938
$h = 1/8$	0.0356	0.0612	0.0347	0.0957	0.0678
$h = 1/16$	0.0093	0.0271	0.0092	0.0631	0.0132
$h = 1/32$	0.0024	0.0171	0.0024	0.0524	0.0033
$h = 1/64$	0.0006	0.0145	0.0006	0.0520	0.0115

(d)

	$\gamma = -45°$	$\gamma = -22.5°$	$\gamma = 0°$	$\gamma = +22.5°$	$\gamma = +45°$
$h = 1/4$	0.0165	0.0521	0.0173	0.0849	0.1156
$h = 1/8$	0.0052	0.0222	0.0047	0.0324	0.0481
$h = 1/16$	0.0007	0.0052	0.0007	0.0108	0.0192
$h = 1/32$	0.0005	0.0014	0.0007	0.0033	0.0038
$h = 1/64$	0.0000	0.0003	0.0000	0.0009	0.0013

(e)

Table 4: Total energy (column 1 in Table 1) (a) for the conforming element with exact boundary conditions, (b) for the conforming element with relaxed boundary conditions, (c) for the classical non-conforming element with exact boundary conditions, (d) for the classical non-conforming element with relaxed boundary conditions, (e) for the discontinuous element.

	$\gamma = -45°$	$\gamma = -22.5°$	$\gamma = 0°$	$\gamma = +22.5°$	$\gamma = +45°$
$h = 1/4$	0.0733	0.0890	0.0980	0.1068	0.0800
$h = 1/8$	0.0773	0.0832	0.1171	0.0904	0.1043
$h = 1/16$	0.0459	0.0574	0.0658	0.0685	0.0857
$h = 1/32$	0.0243	0.0309	0.0345	0.0452	0.0648
$h = 1/64$	0.0125	0.0158	0.0177	0.0274	0.0308

(a)

	$\gamma = -45°$	$\gamma = -22.5°$	$\gamma = 0°$	$\gamma = +22.5°$	$\gamma = +45°$
$h = 1/4$	0.1882	0.1997	0.1897	0.1838	0.1975
$h = 1/8$	0.1004	0.1433	0.1398	0.1363	0.1208
$h = 1/16$	0.0509	0.0653	0.0717	0.0855	0.0590
$h = 1/32$	0.0255	0.0325	0.0360	0.0441	0.0276
$h = 1/64$	0.0128	0.0162	0.0180	0.0185	0.0122

(b)

	$\gamma = -45°$	$\gamma = -22.5°$	$\gamma = 0°$	$\gamma = +22.5°$	$\gamma = +45°$
$h = 1/4$	0.1055	0.1332	0.1708	0.1405	0.1194
$h = 1/8$	0.0857	0.0954	0.1196	0.0957	0.0765
$h = 1/16$	0.0473	0.0586	0.0662	0.0585	0.0424
$h = 1/32$	0.0246	0.0315	0.0346	0.0313	0.0241
$h = 1/64$	0.0125	0.0162	0.0177	0.0163	0.0125

(c)

	$\gamma = -45°$	$\gamma = -22.5°$	$\gamma = 0°$	$\gamma = +22.5°$	$\gamma = +45°$
$h = 1/4$	0.1864	0.2194	0.1991	0.1980	0.1536
$h = 1/8$	0.1003	0.1468	0.1396	0.1452	0.1137
$h = 1/16$	0.0509	0.0664	0.0716	0.0670	0.0592
$h = 1/32$	0.0255	0.0334	0.0360	0.0337	0.0289
$h = 1/64$	0.0128	0.0167	0.0180	0.0168	0.0135

(d)

	$\gamma = -45°$	$\gamma = -22.5°$	$\gamma = 0°$	$\gamma = +22.5°$	$\gamma = +45°$
$h = 1/4$	0.0960	0.1223	0.1375	0.1301	0.1233
$h = 1/8$	0.0673	0.0915	0.1015	0.0896	0.0728
$h = 1/16$	0.0505	0.0658	0.0718	0.0634	0.0519
$h = 1/32$	0.0351	0.0468	0.0504	0.0458	0.0357
$h = 1/64$	0.0255	0.0332	0.0361	0.0327	0.0251

(e)

Table 5: Error of the deformation in the L^2-norm (column 2 in Table 1) (a) for the conforming element with exact boundary conditions, (b) for the conforming element with relaxed boundary conditions, (c) for the classical non-conforming element with exact boundary conditions, (d) for the classical non-conforming element with relaxed boundary conditions, (e) for the discontinuous element.

	$\gamma = -45°$	$\gamma = -22.5°$	$\gamma = 0°$	$\gamma = +22.5°$	$\gamma = +45°$
$h = 1/4$	0.2665	0.3946	0.4089	0.5459	0.4849
$h = 1/8$	0.3135	0.3942	0.4368	0.4842	0.5063
$h = 1/16$	0.2474	0.3297	0.3086	0.4135	0.4483
$h = 1/32$	0.1834	0.2758	0.2158	0.3446	0.3805
$h = 1/64$	0.1313	0.2330	0.1496	0.3145	0.3255

(a)

	$\gamma = -45°$	$\gamma = -22.5°$	$\gamma = 0°$	$\gamma = +22.5°$	$\gamma = +45°$
$h = 1/4$	0.0173	0.2006	0.0653	0.3002	0.3375
$h = 1/8$	0.0199	0.1975	0.0398	0.2741	0.3216
$h = 1/16$	0.0105	0.1882	0.0137	0.2302	0.3502
$h = 1/32$	0.0037	0.1872	0.0045	0.2324	0.3670
$h = 1/64$	0.0013	0.1880	0.0015	0.2477	0.3886

(b)

	$\gamma = -45°$	$\gamma = -22.5°$	$\gamma = 0°$	$\gamma = +22.5°$	$\gamma = +45°$
$h = 1/4$	0.3547	0.4289	0.5002	0.4291	0.2750
$h = 1/8$	0.3427	0.3598	0.4017	0.3486	0.2356
$h = 1/16$	0.2657	0.2778	0.2813	0.2839	0.2018
$h = 1/32$	0.1945	0.2221	0.1978	0.2313	0.1994
$h = 1/64$	0.1374	0.1690	0.1373	0.1965	0.1551

(c)

	$\gamma = -45°$	$\gamma = -22.5°$	$\gamma = 0°$	$\gamma = +22.5°$	$\gamma = +45°$
$h = 1/4$	0.0419	0.1461	0.0884	0.1922	0.0368
$h = 1/8$	0.0358	0.0982	0.0519	0.1502	0.1573
$h = 1/16$	0.0167	0.0883	0.0194	0.1495	0.0137
$h = 1/32$	0.0063	0.0950	0.0068	0.1509	0.0051
$h = 1/64$	0.0023	0.0961	0.0023	0.1525	0.0630

(d)

	$\gamma = -45°$	$\gamma = -22.5°$	$\gamma = 0°$	$\gamma = +22.5°$	$\gamma = +45°$
$h = 1/4$	0.0097	0.0772	0.0169	0.0635	0.0897
$h = 1/8$	0.0058	0.0484	0.0062	0.0374	0.0471
$h = 1/16$	0.0012	0.0142	0.0011	0.0164	0.0185
$h = 1/32$	0.0008	0.0047	0.0007	0.0063	0.0056
$h = 1/64$	0.0002	0.0015	0.0001	0.0021	0.0020

(e)

Table 6: Error of the deformation gradient in laminate direction in the L^2-norm (column 3 in Table 1) (a) for the conforming element with exact boundary conditions, (b) for the conforming element with relaxed boundary conditions, (c) for the classical non-conforming element with exact boundary conditions, (d) for the classical non-conforming element with relaxed boundary conditions, (e) for the discontinuous element.

	$\gamma = -45°$	$\gamma = -22.5°$	$\gamma = 0°$	$\gamma = +22.5°$	$\gamma = +45°$
$h = 1/4$	0.3125	0.3750	0.2500	0.4375	0.5000
$h = 1/8$	0.1875	0.2344	0.2500	0.2578	0.3125
$h = 1/16$	0.1172	0.1816	0.1250	0.1816	0.2188
$h = 1/32$	0.0645	0.1704	0.0625	0.1455	0.1533
$h = 1/64$	0.0337	0.1477	0.0303	0.1028	0.1326

(a)

	$\gamma = -45°$	$\gamma = -22.5°$	$\gamma = 0°$	$\gamma = +22.5°$	$\gamma = +45°$
$h = 1/4$	0.2500	0.1562	0.0000	0.1562	0.5000
$h = 1/8$	0.0000	0.1484	0.0000	0.1328	0.1562
$h = 1/16$	0.0000	0.1074	0.0000	0.0703	0.1797
$h = 1/32$	0.0000	0.1191	0.0000	0.1055	0.2168
$h = 1/64$	0.0000	0.1234	0.0000	0.1218	0.2324

(b)

	$\gamma = -45°$	$\gamma = -22.5°$	$\gamma = 0°$	$\gamma = +22.5°$	$\gamma = +45°$
$h = 1/4$	0.3125	0.1875	0.2500	0.3438	0.2500
$h = 1/8$	0.0469	0.0859	0.1250	0.2344	0.2031
$h = 1/16$	0.0586	0.0703	0.0625	0.1504	0.2109
$h = 1/32$	0.0381	0.0527	0.0312	0.1216	0.1641
$h = 1/64$	0.0212	0.0326	0.0154	0.1105	0.1029

(c)

	$\gamma = -45°$	$\gamma = -22.5°$	$\gamma = 0°$	$\gamma = +22.5°$	$\gamma = +45°$
$h = 1/4$	0.2500	0.0312	0.0000	0.2188	0.1250
$h = 1/8$	0.0000	0.0078	0.0000	0.0781	0.0156
$h = 1/16$	0.0000	0.0000	0.0000	0.0762	0.0312
$h = 1/32$	0.0000	0.0137	0.0000	0.0869	0.0156
$h = 1/64$	0.0000	0.0144	0.0000	0.0902	0.0134

(d)

	$\gamma = -45°$	$\gamma = -22.5°$	$\gamma = 0°$	$\gamma = +22.5°$	$\gamma = +45°$
$h = 1/4$	0.0000	0.0000	0.0000	0.0000	0.0625
$h = 1/8$	0.0312	0.0547	0.0000	0.0781	0.0312
$h = 1/16$	0.0000	0.0000	0.0000	0.0000	0.0020
$h = 1/32$	0.0186	0.0029	0.0312	0.0049	0.0068
$h = 1/64$	0.0000	0.0000	0.0000	0.0000	0.0000

(e)

Table 7: Error in the volume fraction λ^1 for $\omega = \Omega$ (column 4 in Table 1 with $i = 1$) (a) for the conforming element with exact boundary conditions, (b) for the conforming element with relaxed boundary conditions, (c) for the classical non-conforming element with exact boundary conditions, (d) for the classical non-conforming element with relaxed boundary conditions, (e) for the discontinuous element.

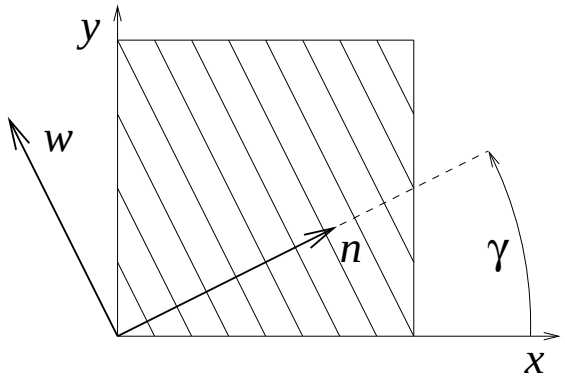

Figure 1: Definition of the vectors n and w as functions of γ.

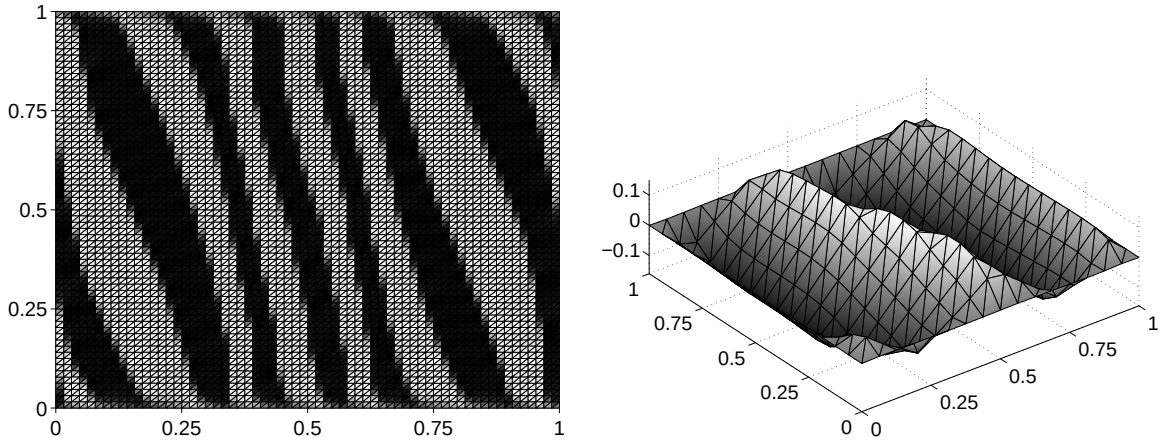

(a) (b)

Figure 2: Conforming element with exact boundary conditions ($\alpha_2 = 1000$) for angle $\gamma = +22.5°$, (a) deformation gradient in normal direction with $h = 1/64$, (b) deformation with $h = 1/16$.

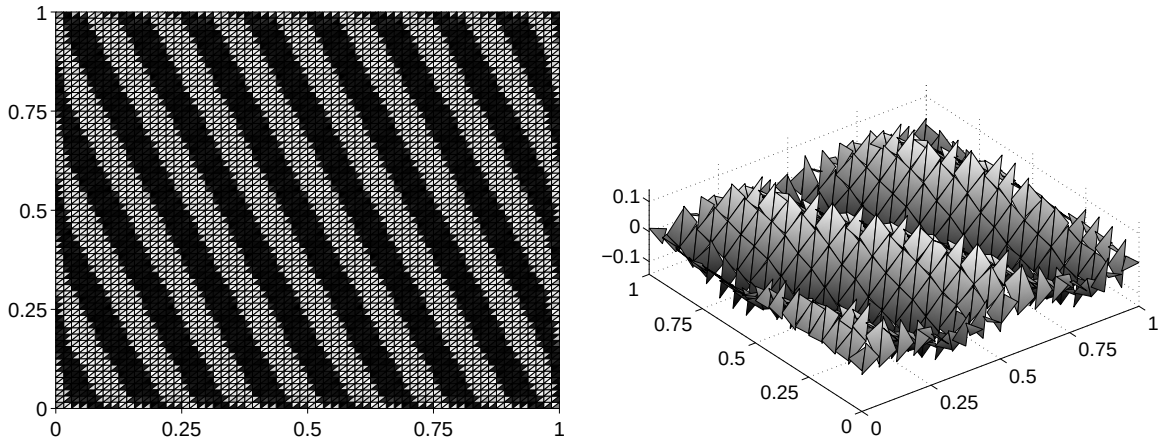

(a) (b)

Figure 3: Classical non-conforming element with exact boundary conditions ($\alpha_2 = 1000$) for angle $\gamma = +22.5°$, (a) deformation gradient in normal direction with $h = 1/64$, (b) deformation with $h = 1/16$.

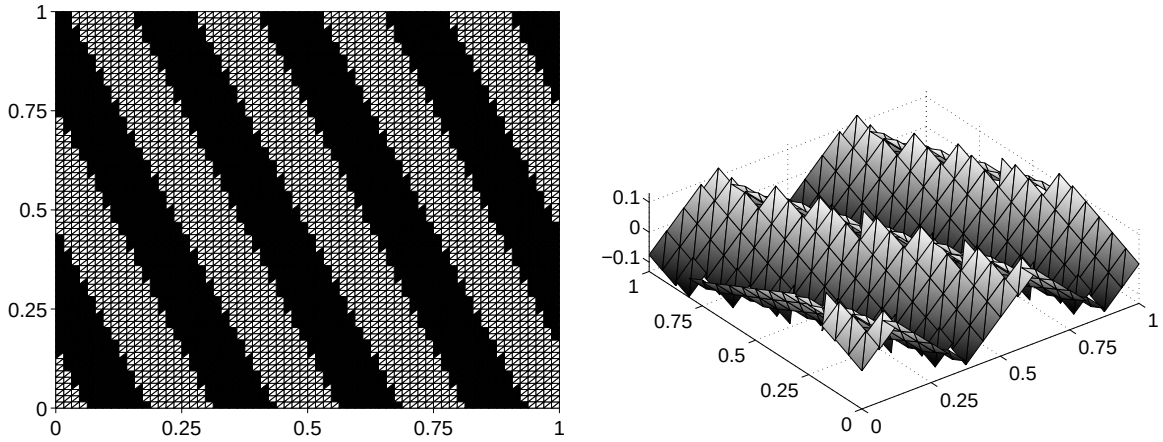

(a) (b)

Figure 4: Discontinuous element with relaxed boundary conditions ($\alpha_2 = 1$) for angle $\gamma = +22.5°$, (a) deformation gradient in normal direction with $h = 1/64$, (b) deformation with $h = 1/16$.

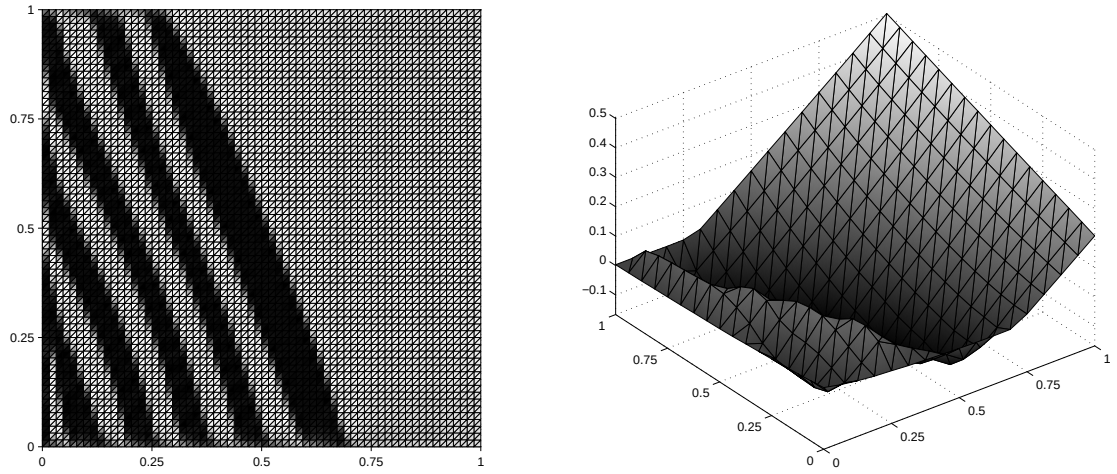

(a) (b)

Figure 5: Conforming element with exact boundary conditions ($\alpha_2 = 1000$), (a) deformation gradient in normal direction with $h = 1/64$, (b) deformation with $h = 1/16$.

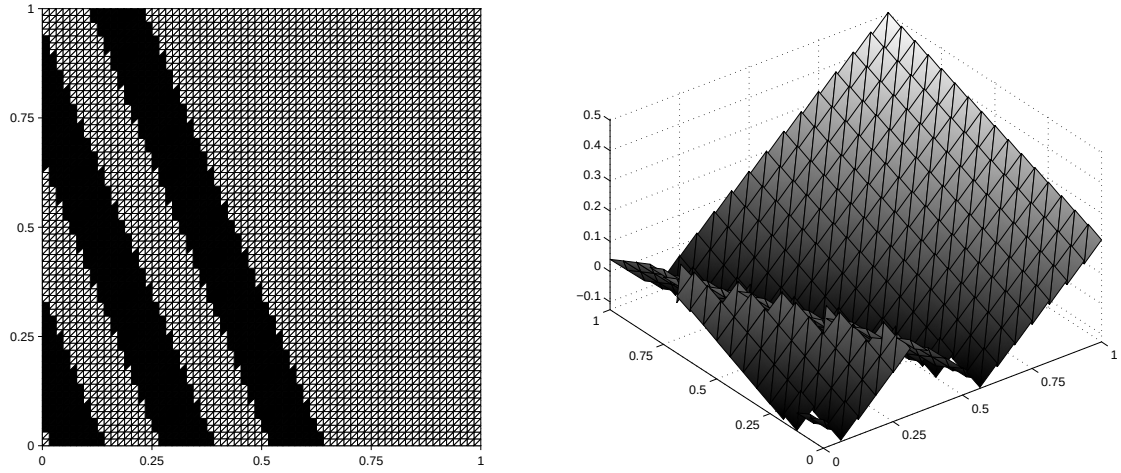

(a) (b)

Figure 6: Discontinuous element with relaxed boundary conditions ($\alpha_2 = 1$), (a) deformation gradient in normal direction with $h = 1/64$, (b) deformation with $h = 1/16$.

References

[1] J. Ball and R. James, *Fine phase mixtures as minimizers of energy*, Arch. Rat. Mech. Anal., 100 (1987), pp. 13–52.

[2] ——, *Proposed experimental tests of a theory of fine microstructure and the two-well problem*, Phil. Tras. R. Soc. Lond. A, 338 (1992), pp. 389–450.

[3] H. Blum, J. Harig, S. Müller, and S. Turek, *FEAT2D: Finite element analysis tools. User manual. Release 1.3*, tech. rep., Universität Heidelberg, 1992.

[4] C. Carstensen and P. Plecháč, *Numerical solution of the scalar double-well problem allowing microstructure*, Math. Comp., 66 (1997), pp. 997–1026.

[5] C. Carstensen and T. Roubíček, *Numerical approximation of young measures in non-convex variational problems*, Tech. Rep. 97-18, Universität Kiel, 1997.

[6] M. Chipot, C. Collins, and D. Kinderlehrer, *Numerical analysis of oscillations in multiple well problems*, Numer. Math., 70 (1995), pp. 259–282.

[7] M. Chipot and S. Müller. private communications.

[8] C. Collins, *Computation and analysis of twinning in crystalline solids*. Ph.D. thesis, University of Minnesota, 1990.

[9] ——, *Comparison of computational results for twinning in the two-well problem*, in Proceedings of the 2nd International Conference on Intelligent Materials, C. Rogers and G. Wallace, eds., Technomic, 1994, pp. 391–401.

[10] B. Dacorogna, *Direct Methods in the Calculus of Variations*, Springer, 1989.

[11] M. K. Gobbert and A. Prohl, *A discontinuous finite element method for solving a multi-well problem*, Tech. Rep. 1539, IMA, 1998.

[12] P. Gremaud, *Numerical analysis of a nonconvex variational problem related to solid-solid phase transitions*, SIAM J. Numer. Anal., 31 (1994), pp. 111–127.

[13] P. Klouček and M. Luskin, *The computation of the dynamics of martensitic microstructure*, Continuum Mech. Thermodyn., 6 (1994), pp. 209–240.

[14] M. Kružík, *Numerical approach to double well problems*, Tech. Rep. 1485, IMA, 1997.

[15] B. Li and M. Luskin, *Nonconforming finite element approximation of crystalline microstructure*, Tech. Rep. 1420, IMA, 1996.

[16] ——, *Finite element analysis of microstructure for the cubic to tetragonal transformation*, SIAM J. Numer. Anal., 35 (1998), pp. 376–392.

[17] D. G. Luenberger, *Linear and Nonlinear Programming*, Addison-Wesley, second ed., 1989.

[18] M. Luskin, *Approximation of a laminated microstructure for a rotationally invariant, double well energy density*, Numer. Math., 75 (1996), pp. 205–221.

[19] ——, *On the computation of crystalline microstructure*, Acta Numerica, 5 (1996), pp. 191–257.

[20] R. A. Nicolaides and N. J. Walkington, *Strong convergence of numerical solutions to degenerate variational problems*, Math. Comp., 64 (1995), pp. 117–127.

[21] P. Pedregal, *Parameterized Measures and Variational Principles*, Birkhäuser, 1997.

[22] A. Prohl, *An adaptive finite element method for solving a double well problem describing crystalline microstructure*, Tech. Rep. 1542, IMA, 1998.

[23] T. Roubíček, *Relaxation in Optimization Theory and Variational Calculus*, Walter de Gruyter, Berlin, New York, 1997.